

Nucleon Form Factors - A Jefferson Lab Perspective

John Arrington¹, Kees de Jager² and Charles F. Perdrisat³

¹ Physics Division, Argonne National Laboratory, Argonne, IL 60439, USA

² Thomas Jefferson National Accelerator Facility, Newport News, VA 23606, USA

³ College of William and Mary, Williamsburg, VA 23187, USA

E-mail: johna@anl.gov

Abstract.

The charge and magnetization distributions of the proton and neutron are encoded in their elastic electromagnetic form factors, which can be measured in elastic electron–nucleon scattering. By measuring the form factors, we probe the spatial distribution of the proton charge and magnetization, providing the most direct connection to the spatial distribution of quarks inside the proton. For decades, the form factors were probed through measurements of unpolarized elastic electron scattering, but by the 1980s, progress slowed dramatically due to the intrinsic limitations of the unpolarized measurements. Early measurements at several laboratories demonstrated the feasibility and power of measurements using polarization degrees of freedom to probe the spatial structure of the nucleon. A program of polarization measurements at Jefferson Lab led to a renaissance in the field of study, and significant new insight into the structure of matter.

1. Introduction

The electromagnetic form factors encode the spatial distributions of charge and magnetization in the nucleon. In a simple picture, the two form factors of a spin-1/2 object, G_E and G_M , relate to the spatial distribution of charge and magnetization inside the object. In the nucleon, the quarks are the carriers of charge, and so these observables are directly connected to the spatial distribution of quarks in the nucleon, as well as a probe of the underlying dynamics.

In the 1950s electron scattering became the tool of choice for measuring the nucleon form factors. An active program mapped out the form factors as well as possible, but the ability to extract the form factors using unpolarized cross-section measurements was limited. By the 1980s most of the experiments provided only incremental improvements on the precision or on the Q^2 -range of existing measurements, or were early proof-of-principle tests of new techniques.

The advent of electron beams with high luminosity and polarization, combined with new polarized targets, recoil polarimeters, and large-acceptance detectors, led to a revolution in the study of nucleon form factors. In the last 10 years measurements at Jefferson Lab have rewritten the textbook on the proton and neutron form factors. The techniques that have allowed this dramatic resurgence of interest in the form factors have also opened up other possibilities, allowing us to try and isolate the contribution of strangeness in the nucleon and making cleaner and more precise measurements of the impact of the nuclear environment on the internal structure of the proton and neutron.

2. Historical Context

In the Born approximation, where the interaction occurs via the exchange of a single virtual photon, the unpolarized e - N elastic cross section can be written in terms of the Sachs form factors, G_E and G_M , as

$$\frac{d\sigma}{d\Omega} = \frac{\sigma_{Mott}}{\varepsilon(1+\tau)} \left[\tau G_M^2(Q^2) + \varepsilon G_E^2(Q^2) \right], \quad (1)$$

where $\tau = Q^2/4M^2$, $-Q^2$ the square of the four-momentum transfer, M the nucleon mass, and $\varepsilon = 1/[1 + 2(1 + \tau) \tan^2(\theta_e/2)]$ is the linear polarization parameter of the virtual photon. The value of ε depends on the scattering angle θ_e , with $\varepsilon \rightarrow 1$ in the limit of forward scattering, and $\varepsilon = 0$ for 180° scattering. The term σ_{Mott} denotes the cross section for the scattering of two spin-1/2 point-like objects. The quantity in brackets is referred to as the reduced cross section which, at fixed Q^2 , depends only on the values of G_E , G_M , and ε . The electric and magnetic form factors can also be written in terms of the Dirac and Pauli form factors: $G_E = F_1 - \tau F_2$, $G_M = F_1 + F_2$. Writing the cross section in terms of the Sachs form factors (Eq. 1) yields a simpler expression, without the cross terms that appear when using F_1 and F_2 . By performing a Rosenbluth separation - making cross-section measurements at a fixed Q^2 -value but two or more ε -values - one can separate the values of G_E^2 and G_M^2 .

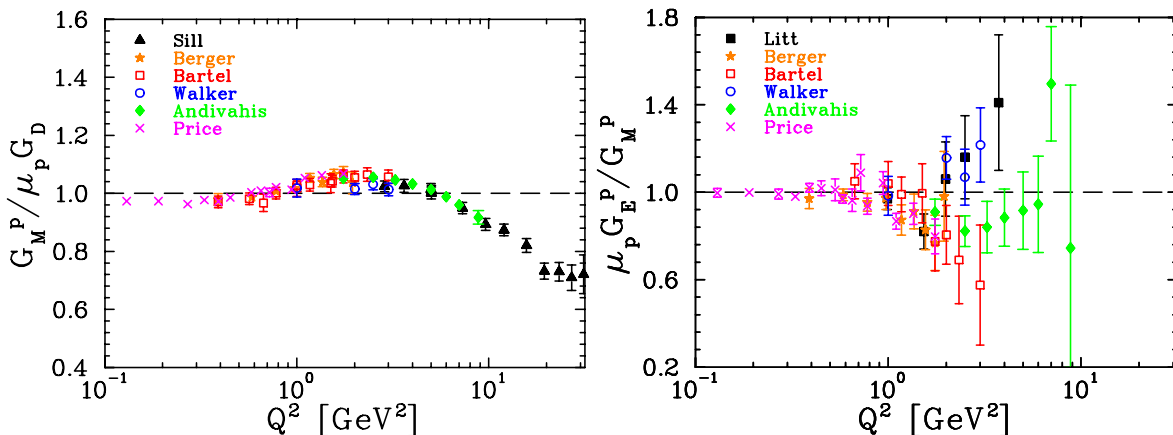


Figure 1. Database for $G_M^p/\mu_p G_D$ (left) and $\mu_p G_E^p/G_M^p$ (right) obtained by the Rosenbluth method as of the mid-1990s.

This technique is limited in its ability to make a clean separation of the form factors. One can see from the form of the reduced cross section that there is very little sensitivity to G_E for $Q^2 \gg 1$ - or for $(G_E/G_M)^2 \ll 1$ - and little sensitivity to G_M for $Q^2 \ll 1$, except for $\theta_e \rightarrow 180^\circ$. Nonetheless, it was possible to make measurements of G_E^p and especially G_M^p over a wide range in Q^2 , as seen in Fig. 1, which shows the status of proton form-factor measurements in the mid-1990s, see [1, 2, 3] for details of the measurements. The Q^2 -dependence of the proton magnetic form factor is well approximated by the dipole form up to 10 GeV^2 ($G_M^p/\mu_p \approx G_D = (1 + Q^2/0.71)^{-2}$ with μ_p the proton magnetic moment), and falls $\sim 30\%$ below the dipole form at $Q^2 \approx 30 \text{ GeV}^2$. While G_E^p was also reasonably well approximated by the dipole form, systematic variations between the results of different experiments were much larger in G_E^p than G_M^p . However, the general conclusion was that the data were consistent with form-factor scaling, i.e. $\mu_p G_E^p/G_M^p$ was independent of Q^2 , up to at least 5 GeV^2 . This was consistent with simple non-relativistic quark models, as well as the perturbative QCD expectation at large Q^2 .

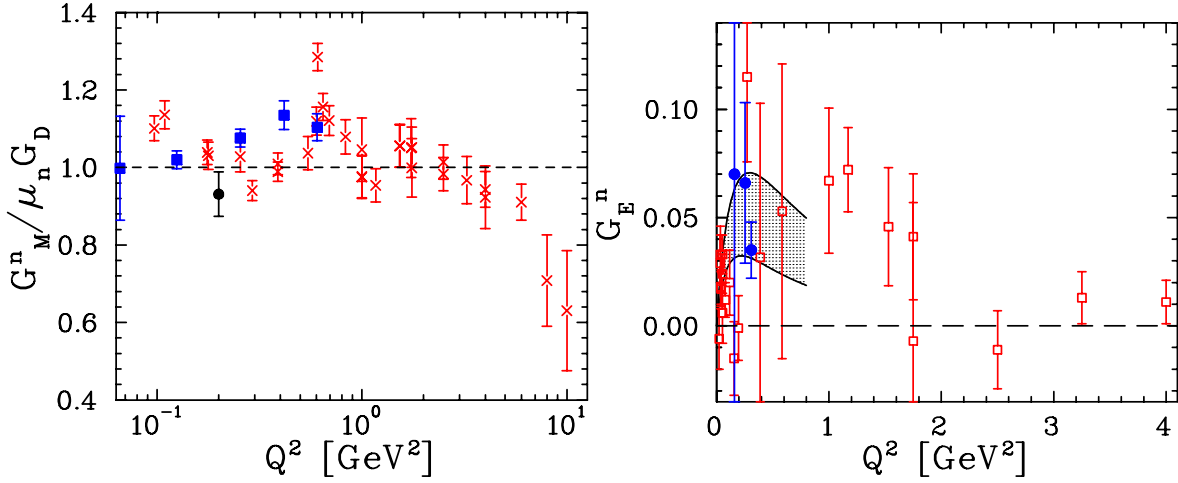


Figure 2. Database for $G_M^n / \mu_n G_D$ (left) and G_E^n (right) before the JLab turn-on. For G_M^n , the crosses are from quasi-elastic scattering (inclusive and coincidence), the solid squares are from ratio measurements, and the solid circle from a polarization experiment. For G_E^n , the solid circles are from polarization measurements, and the hollow squares from quasi-elastic scattering data. The shaded band shows the range of results extracted from a model-dependent analysis of elastic $e-d$ scattering [4].

For the neutron, measurements using the Rosenbluth technique were even more difficult. The need to use light nuclei as “effective” neutron targets necessitated large corrections in extracting the $e-n$ cross section, thus limiting the precision and kinematic coverage for extractions of G_M^n . The extraction of G_E^n was even more problematic, as G_E^n is much smaller than the other electromagnetic form factors. Therefore, there were no precise extractions of G_E^n , and for $Q^2 \gtrsim 2$ GeV² only upper limits could be set. In the limit $Q^2 \rightarrow 0$, G_E^n must approach zero (the charge of the neutron), while at finite Q^2 , any non-zero value must come from a difference in the spatial distribution of up and down quarks in the neutron.

Figure 2 shows the status of neutron form-factor measurements around the time of the JLab turn-on in 1996. For G_E^n , the data are mainly from quasi-elastic scattering from the deuteron and from elastic $e-d$ scattering, which has large model-dependent uncertainties, indicated by the shaded band. Only a few proof-of-principle polarization measurements had been performed. For G_M^n , most of the results are from inclusive quasi-elastic scattering measurements from the deuteron, and the large uncertainties show the impact of the proton subtraction and the nuclear corrections. A few data had been measured using the so-called ratio technique which, along with the polarization measurements, will be described in the following sections.

It had long been known [5, 6, 7, 8] that, in principle, including measurements of polarization observables would allow a much improved determination of the form factors. Using a polarized electron beam, one can measure either the cross-section asymmetry from a polarized target or the polarization transferred to an unpolarized nucleon. In both cases, the measured asymmetry depends only on the ratio G_E/G_M , thus providing sensitivity to the electric form factor even if its contribution to the unpolarized cross section is extremely small. However, it required the development of high intensity, highly polarized electron beams and polarized targets or recoil polarimeters with high figures of merit to apply this theory to advance our knowledge of the form factors.

Already at the third Program Advisory Committee (PAC) meeting of the CEBAF in February of 1989 three letters of intent (LOI) had been presented to measure nucleon form factors with

Table 1. List of JLab experiments related to nucleon form factors. Experiments marked with “†” were focused on two-photon exchange contributions. Proposals are available from “http://www.jlab.org/exp_prog/generated/approved.html”.

Expt.(Hall)	Reaction	Goal, Q^2 -range	Expt.(Hall)	Reaction	Goal, Q^2 -range
E93-027(A)	$p(\vec{e}, e'\vec{p})$	G_E^p , 0.5–3.5	E95-001(A)	${}^3\vec{\text{He}}(\vec{e}, e')$	G_M^n , 0.1–0.6
E99-007(A)	$p(\vec{e}, e'\vec{p})$	G_E^p , 3.5–5.6	E94-017(B)	${}^2\text{H}(e, e'N)$	G_M^n , 1–4.8
E04-108(C)	$p(\vec{e}, e'\vec{p})$	G_E^p , 2.5–8.5	E93-026(C)	${}^2\vec{\text{H}}(\vec{e}, e'n)$	G_E^n , 0.5–1.0
E04-019(C)	$p(\vec{e}, e'\vec{p})^\dagger$	G_E^p , 2.5	E93-038(C)	${}^2\text{H}(\vec{e}, e'\vec{n})$	G_E^n , 0.4–1.5
E01-001(A)	$p(e, e'p)^\dagger$	G_E^p , 2.6–4.1	E02-013(A)	${}^3\vec{\text{He}}(\vec{e}, e'n)$	G_E^n , 1.4–3.4
E05-017(C)	$p(e, e'p)^\dagger$	G_E^p , 0.4–5.8	E04-110(C)	${}^2\text{H}(\vec{e}, e'\vec{n})$	G_E^n , 4.3
E08-007(A)	$p(\vec{e}, e'\vec{p})$	G_E^p , 0.25–0.7	E07-005(B)	$p(e^\pm, e'p)^\dagger$	TPE, 0.5–3.0
E08-007(A)	$\vec{p}(\vec{e}, e'p)$	G_E^p , 0.015–0.4			

the new techniques being developed; two to measure G_E^n and one to measure G_E^p . These LOIs were then developed into full-blown proposals, resulting in five fully approved proposals in 1994, shortly before the start of operations. The first experiments provided much improved measurements of proton and neutron form factors, as well as some unexpected and exciting results. This led to a variety of proposals, summarized in Table 1, aimed at fully developing and exploiting these new techniques to extend the kinematic coverage and precision of the data. Within a decade of the first measurement, this program would drastically transform our state of understanding of nucleon form factors. Related measurements examining parity-violating elastic scattering as well as meson and transition form factors are discussed in other reviews in this collection.

3. Proton Form Factors

The original motivation for the new measurements of the proton electric form factor was the internal inconsistency of the database of the time, which showed a rapid increase in the uncertainty and scatter of the results with Q^2 , starting at $\sim 1 \text{ GeV}^2$; see Fig. 1. The initial experiment in Hall A yielded unexpected results, which created significant excitement in the field. A great deal of effort went into trying to understand the implications of the new data on our picture of the proton, and to extend the polarization measurements to higher Q^2 -values. There was also significant activity aimed at understanding the discrepancy with previous measurements, and making significant improvements in precision at low Q^2 -values.

First, we discuss the new techniques that made such measurements feasible, then we present the results of the initial high- Q^2 experiments, as well as the later studies that were an offshoot of these new techniques.

3.1. Techniques

Polarization-transfer experiments measure the polarization of the recoiling proton by re-scattering it in an appropriate material and determining the resulting azimuthal asymmetry distribution, thus providing a measurement of the two components of the polarization in a plane perpendicular to the proton momentum. After being struck by a polarized electron, the proton has in-plane polarization components parallel (P_ℓ) and perpendicular (P_t) to the proton momentum. The component normal to the scattering plane is zero in the Born approximation. To measure both P_ℓ and P_t simultaneously requires precession of P_ℓ into a normal component, using a dipole magnet. The precession in the dispersive plane of a dipole is given by $\chi = \gamma \cdot (\theta_B + \theta_{target} - \theta_{fpp}) \cdot \kappa_p$, where γ , θ_B , θ_{target} , θ_{fpp} and $\kappa_p = \mu_p - 1$ are the proton’s relativistic factor, the mean bending angle of the dipole, the entrance and exit angle of

an individual proton trajectory, and the anomalous proton magnetic moment, respectively. The resulting distribution in the azimuthal angle φ is

$$N(\vartheta, \varphi) = N_0 \cdot [1 + h(P_b A_y(\vartheta) P_n^{fpp} \sin \varphi - P_b A_y(\vartheta) P_t^{fpp} \cos \varphi)], \quad (2)$$

where N_0 is the average number of events in a given interval of θ and φ , P_b is the electron beam longitudinal polarization and $h = \pm 1$ the helicity state of the beam, and $P_n^{fpp} \approx P_\ell \sin \chi$ and $P_t^{fpp} \approx P_t$ are the polarization components in the polarimeter; $A_y(\vartheta)$ is the analyzing power at a given polar scattering angle ϑ . The relative beam-helicity difference distribution in a given ϑ interval is then:

$$\frac{N^{h=+1}(\varphi) - N^{h=-1}(\varphi)}{2N_0} = P_b A_y (P_n^{fpp} \sin \varphi - P_t^{fpp} \cos \varphi) \quad (3)$$

Taking only the spin precession in the dispersive plane, χ , into account, the ratio $P_t^{fpp} \sin \chi / P_n^{fpp}$ is directly related to the ratio P_t/P_ℓ at the target, which in turn is a measure of G_E^p/G_M^p :

$$\frac{G_E^p}{G_M^p} = -\frac{P_t}{P_\ell} \frac{(E_e + E_{e'})}{2M} \tan(\theta_e/2) = -\frac{P_t}{P_\ell} \sqrt{\frac{\tau(1+\varepsilon)}{2\varepsilon}} \quad (4)$$

As G_E^p/G_M^p is defined by the ratio of two polarization components, knowledge of the beam polarization and polarimeter analyzing power is not necessary. The remaining source of systematic uncertainty comes from the accuracy of the spin transport, i.e. the calculation of the components of the polarization at the target from the asymmetry in the focal plane. As Q^2 increases, the precession in the non-dispersive plane due to focusing elements in the spectrometer becomes significant and has to be taken into account. This residual systematic uncertainty can be evaluated on the basis of optical studies [9].

In almost all recoil-polarization experiments at JLab, both final-state particles were detected to reduce the inelastic contamination. The first focal-plane polarimeter (FPP) built in Hall A was used for the GEp(I) experiment, E93-027 [10, 9]. Several changes were required to utilize the full beam energy of the accelerator and extend the measurements to higher Q^2 . For a fixed beam energy, the cross section scales as Q^{-12} and the analyzing power decreases with increasing Q^2 . Furthermore, the electron solid angle matching the proton acceptance increases with Q^2 . To compensate for these factors in GEp(II) (E99-007), the electron was detected in a large solid-angle electromagnetic calorimeter, and the polarimeter was reconfigured with 95 g/cm² of CH₂ instead of graphite to increase the effective analyzing power.

As the maximum momentum of the proton spectrometer in Hall A limited the range of possible Q^2 , GEp(III) (E04-018) used the HMS spectrometer in Hall C, which can detect proton momenta up to 7.5 GeV/c. To increase the figure of merit at high Q^2 , a new FPP was built, consisting of two polarimeters in succession, each containing a slab of polyethylene, 50 g/cm² thick, followed by a set of drift chambers. A larger calorimeter (“BigCal”) was needed to match the proton acceptance at these large Q^2 -values. An entirely new calorimeter was built, consisting of 1744 lead glass bars 4×4 cm² in cross section, and 40-45 cm long, with a frontal area of 2.6 m². A trigger signal from the calorimeter was required for the definition of an $(e, e'p)$ or an $(e, \gamma p)$ event.

3.2. High- Q^2 regime

GEp(I) ran in mid-1998 and measured the G_E^p/G_M^p ratio up to 3.5 GeV² [9]. The results, shown in Fig. 3, revealed an unexpected decrease of G_E^p/G_M^p with increasing Q^2 , in disagreement with scaling. When GEp(II) extended the measurement of G_E^p/G_M^p to 5.6 GeV², the ratio was found

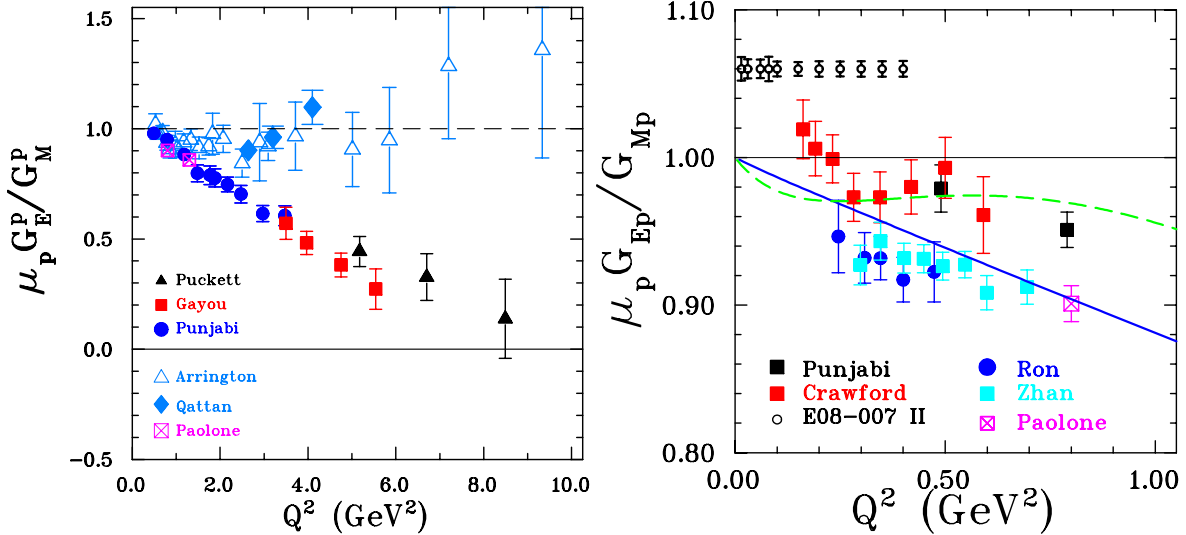


Figure 3. Left: The ratio $\mu_p G_E^p / G_M^p$ from JLab and MIT-Bates (BLAST) polarization experiments, a global analysis of cross-section measurements [13] (hollow triangles), and the “Super-Rosenbluth” results [14] (solid diamonds). Right: Focus on the low- Q^2 results from polarization measurements [9, 15, 16, 17, 18], and projections for the polarized target measurement of E08-007. The dashed green line is the fit of Kelly [19], made before most of these data were available, and an updated [17] version of the fit from Ref. [20].

to continue to decrease linearly with Q^2 , to a value of $\mu_p G_E^p / G_M^p = 0.28 \pm 0.09$ at 5.6 GeV^2 [11]. The GEp(III) measurement extended the measurements up to 8.5 GeV^2 [12], with the data suggesting a slower decrease of the ratio G_E^p / G_M^p above $5\text{--}6 \text{ GeV}^2$.

The results from polarization transfer and Rosenbluth extraction of G_E^p / G_M^p are compared in Fig. 3. The discrepancy between the two results is significant over a wide range of Q^2 . A detailed reanalysis of the world’s cross-section data [21] showed that the apparent discrepancy between different extractions of G_E^p (Fig. 1) was the result of neglecting normalization uncertainties when combining data from different measurements, but that these uncertainties could not account for the systematic difference between Rosenbluth and polarization-transfer results.

Following the unexpected results of the first polarization-transfer experiment, a new Rosenbluth separation of unprecedented accuracy was prepared and the experiment, E01-001, obtained data in 2002. The unique feature of this “Super-Rosenbluth” experiment was the detection of the proton, (e, p) , yielding fixed proton momentum for a given Q^2 , minimal variation of rate as a function of angle, and smaller ε -dependent corrections than (e, e') . This, combined with smaller radiative corrections, led to significantly reduced uncertainties in the ratio G_E^p / G_M^p . The results [14] (solid diamonds in Fig. 3) cover a Q^2 -range from 2.6 to 4.1 GeV^2 , and agree with the previous Rosenbluth extractions. At the same time, traditional Rosenbluth measurements in Hall C [22] provided additional measurements, albeit with much larger uncertainties (these data are included in the global analysis). At that point it was clear that there was a systematic difference between Rosenbluth and recoil-polarization data.

Intensive discussion of various possible explanations followed. With the exception of two-photon exchange (TPE) contributions, radiative corrections were believed to be well understood for the unpolarized case, and small in the relevant polarization observables [23]. Historically, only the IR-divergent component of the TPE corrections had been taken into account. The remaining TPE terms had been evaluated in a soft-photon approximation [24], and found

to be small but potentially important at large Q^2 -values. While the TPE contributions are small, the contribution from G_E^p decreases rapidly as Q^2 increases, and so the TPE corrections can be important in understanding the discrepancy. It was later shown that a ε -dependent correction of $\sim 5\%$ could bring the Rosenbluth results in agreement with the polarization measurements [25, 13], while having little impact on the polarization-transfer results. The status of these studies and of new experiments designed to measure two-photon exchange contributions are discussed in Sec. 3.4.

3.3. Low- Q^2 regime

The Q^2 -region below 1 GeV² is of interest because it covers the range over which the pion cloud is believed to make a significant contribution to the electromagnetic structure of the proton and the neutron. While this yields a significant part of the neutron’s electric form factor at small Q^2 , it is also expected to be important for the form factors of the proton, as discussed for example by Friedrich and Walcher [26]. Extremely low values of Q^2 are interesting because the form-factor behavior as $Q^2 \rightarrow 0$ is connected to the nucleon charge and magnetic radii.

While the neutron was the focus of early measurements at low Q^2 , the demonstration that extremely precise measurements of G_E^p/G_M^p were possible led to improved low- Q^2 measurements of the proton form factor. In recent years careful studies of the optical properties of the Hall A HRS spectrometers have resulted in a significant reduction of the systematic errors in polarization-transfer data, thus allowing measurements of G_E^p/G_M^p below ~ 1 GeV² with a total error of 1% or less. New data from Bates [15], along with updated results [18] from JLab ‘LEDEX’ experiment E05-013 [27] and preliminary results from the dedicated E08-007 measurements [17], are shown in the right panel of Fig. 3. These high precision data do not show any indication of structure in the low- Q^2 ‘‘pion cloud’’ region, although there is at present a systematic disagreement between the polarized target data from Bates [15] and the high precision JLab polarization data [18, 17]. New results from an extensive set of cross section measurements at low Q^2 from Mainz [28] also see a reduction in $\mu_p G_E/G_M$ in this region, consistent with the new JLab data, although they only provide a fit to the form factors, rather than direct extractions of G_E and G_M . Phase II of E08-007 will make extremely high precision measurements using a polarized target. This will provide another comparison between the polarized target and recoil polarization measurements, and will extend the low- Q^2 data down to $Q^2 = 0.015$ GeV². This will allow for significantly improved extractions of the magnetic form factor at very low Q^2 , where the cross section has greatly reduced sensitivity.

Knowledge of the form factors is also important in the analysis of a range of other experiments. Good knowledge of the e - N scattering cross section is crucial to the interpretation of high-precision quasi-elastic scattering measurements aimed at understanding nucleons in nuclei. They are also necessary input to the analysis of parity-violating electron scattering, where the contributions from strange quarks can be isolated given sufficient precision on the electromagnetic form factors and the parity-violating asymmetry. In addition, a better determination of the charge and magnetic radii provides input for the hadronic corrections to the hyperfine structure of hydrogen.

3.4. Two-photon exchange

After the observation of a large discrepancy between Rosenbluth and polarization measurements of $\mu_p G_E/G_M$, two-photon exchange corrections received a great deal of attention as a possible explanation. In 2003, two papers, appearing back-to-back in PRL, shed significant light on the issue. The first paper [25] provided a general formalism for scattering beyond the Born approximation, while the second [29] provided a direct calculation of the TPE correction, including the case of two hard photons, calculated in a hadronic basis.

The analysis of Guichon and Vanderhaeghen [25] not only provided the general formalism, but also demonstrated that relatively small TPE contributions might bring the Rosenbluth results into agreement with the new polarization data. They were able to resolve the discrepancy with TPE amplitudes at the 2–3% level, consistent with the expectation of order α_{EM} corrections for higher-order electromagnetic diagrams. These TPE corrections, derived based on a set of very simple assumptions, were, however, at odds with the measured cross-section ratio of positron-proton and electron-proton scattering [30]. A later analysis [31] used modified assumptions to extract a set of TPE amplitudes of similar magnitude that could explain the discrepancy between Rosenbluth and polarization-transfer measurements while being consistent with the comparison of electron and positron data. Because the impact of the TPE corrections is much smaller for polarization transfer measurements, the impact of TPE on the neutron form factors is also small. Rosenbluth extractions of G_M^n were not very precise, and all precision extractions of G_E^n were based on polarization measurements. The recent measurement of the ε dependence of the polarization observables [32] allows a more detailed extraction of the TPE amplitudes [33, 34]. There is still model dependence in the ε dependence of the TPE amplitudes is not fully constrained, but the inclusion of the polarization observables provides additional important constraints.

Following the initial calculation of TPE corrections in a hadronic model, several other theoretical calculations of the two hard-photon exchange contribution were undertaken (see [35]). A difficulty arises from the fact that in the intermediate state inside the box diagram, the proton can be any excited baryon compatible with angular momentum and parity conservation. One approach, expected to be reliable at lower Q^2 , has been to start with a calculation for an unexcited hadron in the intermediate state [29, 36], and then estimate the effect of higher resonance states [37]. Another approach focuses on the high-energy region [38, 39], assuming that the virtual photon interacts with one valence quark and that the residual system of quarks and gluons is accurately described by Generalized Parton Distributions (GPDs). These two approaches yield qualitatively similar behavior: small corrections to polarization observables and a small change in the ε -dependence of the cross section. This change in the ε -dependence results in a large correction to the Rosenbluth extraction of G_E^p at high Q^2 , where the initial ε -dependence is extremely small.

While much of the focus has been on improving the calculation of TPE diagrams, there have also been efforts to improve the treatment of higher-order terms in the radiative corrections [24, 40, 41, 42]. For example, hard Bremsstrahlung terms yield an additional $\sim 1\%$ difference between high and low ε values [42] that is not present in the soft-photon approximation. However, as with most of these comparisons, the result is compared to Mo and Tsai radiative corrections [43]. While this is the general approach adopted in nearly all experimental extractions of the cross sections, many analyses have applied improved corrections, e.g. for multi-photon bremsstrahlung, and further work is required to determine to what extent the corrections actually applied to the data differ from the new calculations.

While the reduced cross section must depend linearly on ε in the Born approximation, TPE contributions will introduce a curvature in the ε -dependence of the cross section (in the Rosenbluth procedure). A global analysis of Rosenbluth measurements set tight limits on the non-linear contributions to the ε -dependence of the cross section [44], but these limits are not tight enough to rule out the non-linear contributions predicted by most TPE calculations. New measurements of the kinematical dependence of the G_E^p/G_M^p ratio, obtained in recoil polarization at a constant Q^2 of 2.48 GeV² in Hall C (E04-019), show no ε -dependence within the statistical uncertainty [45], supporting the calculations that conclude that polarization measurements are not significantly affected by TPE. The most direct test of TPE contributions, the comparison of positron and electron scattering, yields evidence for a non-zero TPE contribution at the 3σ level [30]. At the present time there is no definitive experimental evidence that TPE

contributions are the major cause of the difference between Rosenbluth and recoil-polarization extractions of the proton form factor, although preliminary results from positron-electron comparisons at Novosibirsk [46] yield an excess positron cross section consistent with TPE calculations, and data taking has begun for E07-005, a much more extensive set of comparisons in Hall B.

There is an active program at JLab to determine if TPE corrections do in fact fully explain the discrepancy, and to map out their impact on both the cross section and polarization observables. In Hall C, E05-017 extended the high-precision ‘‘Super-Rosenbluth’’ measurements, covering a large range in Q^2 and ε to better map out the Rosenbluth-polarization difference and to improve the limits on non-linear contributions by a factor of two or more over a wide range in Q^2 . The discrepancy has motivated experiments to compare positron and electron scattering at Novosibirsk, DESY, and Jefferson Lab [47]. Data taking has begun for E07-005, which will provide a new comparison of the e^+p and e^-p cross sections over a broad kinematic range. This experiment is running in Hall B using a tertiary beam of both positrons and electrons over a broad range of energies. This will allow a quantitative study of TPE contributions over a range of ε for Q^2 up to 2–3 GeV², and will directly determine whether TPE corrections fully explain the discrepancy between Rosenbluth and polarization measurements in this region. While G_E^p is a unique case where these small corrections have a large impact on the interpretation of the results, TPE effects contribute to all electron-scattering measurements. A stringent test of the calculations is important to ensure that these corrections are well understood for future measurements that aim for extremely high precision in a variety of reactions.

4. Neutron Form Factors

For the neutron, form-factor extractions using the Rosenbluth technique were limited by the small size of the electric form factor and the need to measure $e-n$ scattering using quasi-elastic scattering from deuteron targets. As discussed in Sec. 2, it was known that G_E^n was positive, but there was a factor of two uncertainty in the values derived from elastic electron–deuteron scattering. While the situation for G_M^n was better, both the precision and Q^2 -range were limited compared to measurements on the proton.

The availability of high-polarization beams, effective polarized-neutron targets, and large neutron detectors and recoil polarimeters made it possible to dramatically improve our knowledge of the neutron form factors. Experiments at other labs had demonstrated the feasibility of such measurements, and begun the process of validating the techniques through comparisons of measurements utilizing different techniques or different target nuclei. The JLab program added to these studies by expanding precision measurements of G_M^n above $Q^2=1$ GeV² and by providing essentially all of the direct measurements of G_E^n above 0.8 GeV².

4.1. Neutron magnetic form factor

Figure 4 shows the present status of measurements of the neutron magnetic form factor. In the high- Q^2 regime, E94-017 [51] completed a study of G_M^n at Q^2 up to ~ 5 GeV² in 2000 by measuring the exclusive neutron/proton cross-section ratio from the deuteron with the CLAS detector in Hall B. The ratio of the ${}^2\text{H}(e, e'n)$ and ${}^2\text{H}(e, e'p)$ reactions in quasi-elastic kinematics is approximately equal to the ratio of elastic scattering off a free neutron and proton, respectively:

$$R_D = \frac{\frac{d\sigma}{d\Omega} [{}^2\text{H}(e, e'n)_{QE}]}{\frac{d\sigma}{d\Omega} [{}^2\text{H}(e, e'p)_{QE}]} = a \cdot R_{free} = a \cdot \frac{\tau(G_M^n)^2 + \varepsilon(G_E^n)^2}{\tau(G_M^p)^2 + \varepsilon(G_E^p)^2} \quad (5)$$

The correction factor a is close to unity for quasi-elastic kinematics and larger Q^2 -values and can be accurately calculated [52] as a function of Q^2 and θ_{pq} , the angle between the momentum transfer and the knocked-out nucleon in the center of mass, using standard models for the

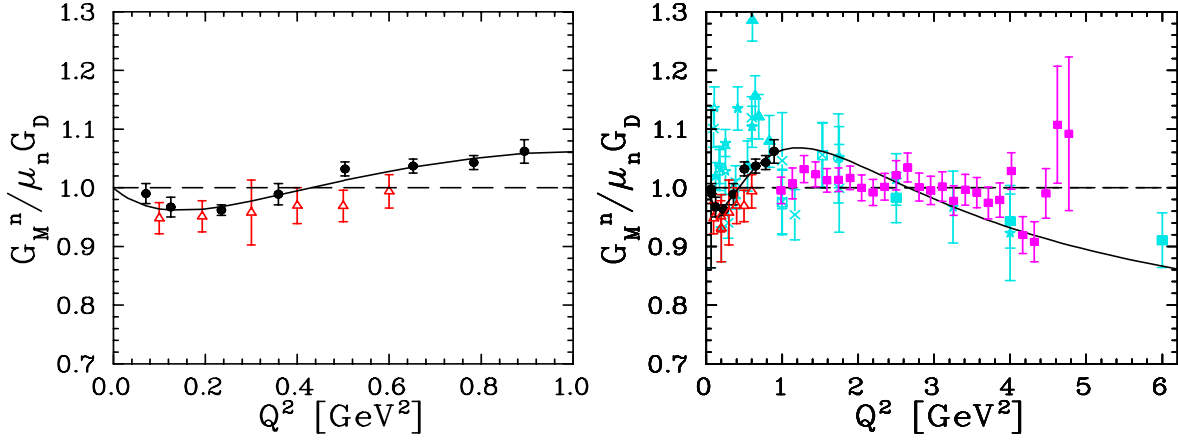


Figure 4. Current status of extractions of $G_M^n/\mu_n/G_D$. The left figure shows only the high precision, low Q^2 JLab polarization [48] (open triangle) and Mainz ratio [49, 50] (closed circles) measurements, while the right figure shows the full data set, including the CLAS ratio [51] measurements (solid squares).

deuteron. The value of G_M^n is then determined from the measured value of R_D and the known values of G_M^p and G_E^p , with very small corrections due to the lack of knowledge of G_E^n . The cross sections for the ${}^2\text{H}(e, e'n)$ and ${}^2\text{H}(e, e'p)$ reactions were measured simultaneously. Measuring the ratio R_D reduces or completely eliminates several systematic uncertainties, such as those from final-state interactions in the deuteron, from knowledge of the luminosity and from radiative corrections. The remaining major uncertainty was due to the neutron detector efficiency, which was measured through pion electroproduction off a hydrogen target. These efficiency measurements were performed simultaneously with the primary deuteron measurement, by positioning a hydrogen target upstream of the deuterium target. The experiment took data at two different beam energies, and for each energy independently analyzed neutrons detected in time-of-flight scintillators and neutrons detected in the calorimeter, yielding four essentially independent but overlapping measurements [51].

Experiment E95-001 [53, 54, 48] determined G_M^n in 1999 at Q^2 -values smaller than 1 GeV^2 by measuring the beam asymmetry in inclusive quasi-elastic scattering of electrons off a polarized ${}^3\text{He}$ target in Hall A. The polarized ${}^3\text{He}$ target system in Hall A utilizes the spin exchange between optically pumped alkali-metal vapor and noble-gas nuclei to produce an ensemble of spin-polarized ${}^3\text{He}$ nuclei. Polarized ${}^3\text{He}$ nuclei serve as an effective polarized neutron target, because their ground state is dominated by a spatially-symmetric s -state in which the spins of the protons cancel. The central feature of the target system is a sealed glass cell, that contains an admixture of ${}^3\text{He}$ gas at a pressure of 0.7 MPa and an alkali-metal vapor. These cells have two chambers, a heated upper chamber in which the spin exchange takes place and a lower one, through which the electron beam passes. Lower cells with lengths from 20 to 40 cm have been used, corresponding to a target thickness of up to $1 \cdot 10^{22} \text{ nuclei/cm}^2$. In earlier versions of the target only rubidium was used as the spin-exchange medium, resulting in an in-beam polarization of up to $\sim 40\%$ at a beam current of up to $\sim 10 \mu\text{A}$. A detailed description of the polarized ${}^3\text{He}$ target system can be found in Ref. [55].

The beam-target asymmetry is:

$$A = -\frac{(\cos \theta^* v_{T'} R_{T'} + 2 \sin \theta^* \cos \phi^* v_{TL'} R_{TL'})}{v_L R_L + v_T R_T}, \quad (6)$$

where θ^* and ϕ^* are the polar and azimuthal target polarization angles with respect to \vec{q} , R_i

denote various nucleon response functions, and v_i the corresponding kinematic factors. By orienting the target polarization parallel to \vec{q} , one measures the ratio of $R_{T'}$ to the unpolarized cross section. In quasi-elastic kinematics $R_{T'}$ is dominantly sensitive to $(G_M^n)^2$:

$$R_{T'} \propto P_n(G_M^n)^2 + P_p(G_M^p)^2, \quad (7)$$

where P_n and P_p denote the effective polarizations of the neutron and the proton, respectively. The extraction of G_M^n requires an iterative process since the asymmetry depends on both $R_{T'}$ and the unpolarized cross section, which also depends strongly on G_M^n . In addition, corrections for the nuclear medium [56] are necessary to take into account effects of final-state interactions and meson-exchange currents. Such corrections are calculable non-relativistically at low Q^2 [53]. At intermediate Q^2 , relativistic effects have to be taken into account, making calculations much more difficult. However, there the size of the corrections is expected to be small and they have been neglected in the analysis [54]. Both measurements are in good agreement in the overlap region (Fig. 4) and with the CLAS data in the larger Q^2 -range, but disagree significantly from earlier Mainz measurements [49, 50], that used the same ratio method as the CLAS measurement, but with an off-site neutron detector calibration.

4.2. Neutron charge form factor

The same techniques that have been used to measure G_E^p/G_M^p can also be applied to measure G_E^n/G_M^n , except that one measures scattering from neutrons in ^2H or ^3He . In the past decade, a series of JLab beam-asymmetry measurements of neutron knock-out from a polarized target or studies of polarization transfer have provided accurate data on G_E^n . The first such measurements at JLab were carried out in Hall C.

Arnold, Carlson and Gross [8] were the first to show that the measurement of the up-down asymmetry in a neutron polarimeter after the spin of the knocked-out neutron has been precessed by a vertical dipole field yields access to the ratio G_E^n/G_M^n . This was the technique used by experiment E93-038, which in 2000 used a large scintillator neutron polarimeter to determine G_E^n at Q^2 -values of 0.45, 1.13 and 1.45 GeV^2 [57]. The neutron polarimeter consisted of a large dipole magnet with a vertically oriented field, an active analyzer (preceded and followed by a veto/tagger), and a top and bottom array of scintillators. The dipole magnet precesses the spin of the neutrons through an angle χ in the horizontal plane and sweeps protons and other charged particles out of the acceptance. The active analyzer consists of twenty $100 \times 10 \times 10 \text{ cm}^3$ scintillators. The long axes were oriented horizontally, perpendicular to the central flight path, stacked vertically into four layers of five detectors. The up/down rear arrays of scintillators each consisted of 12 detectors stacked in three horizontal layers with the long axes of the scintillators oriented parallel to the flight path of the neutrons. The up-down scattering asymmetry measured in this rear array is proportional to the projection of a recoil polarization on to a horizontally-oriented sideways axis. Additional elements of this polarimeter were a lead curtain, veto taggers and extensive steel and concrete shielding surrounding the scintillator detectors [58].

The precession through an angle χ results in a scattering asymmetry $\xi(\chi)$

$$\xi(\chi) = A_y P^n \sin(\chi - \delta) \quad (8)$$

The ratio G_E^n/G_M^n can be determined from the value of the precession angle where the polarization asymmetry is observed to be zero:

$$\frac{G_E^n}{G_M^n} = -\sqrt{\frac{\tau(1 + \varepsilon)}{2\varepsilon}} \tan \delta. \quad (9)$$

By determining a so-called cross-ratio of the up-down asymmetry in the polarimeter for both values of the beam helicity the result becomes independent of both the target luminosity and

the polarimeter efficiency. Corrections for charge-exchange reactions in the lead curtain were determined to be $\approx 3\%$ based on measurements with a liquid hydrogen target and detailed Monte-Carlo simulations.

E93-026 ran in 2001 and used a deuterated ammonia (ND_3) target as an effective polarized neutron target to measure G_E^n at Q^2 of 0.5 and 1.0 GeV^2 [59]. The solid polarized target used the dynamical nuclear polarization technique [60, 61] to reach an in-beam polarization of $\sim 24\%$ at electron beam intensities of up to 100 nA. Ammonia ND_3 granules, doped by radiation damage with a small concentration of free radicals, were immersed in liquid helium. Because the occupation of the magnetic substates in the radicals follow a Boltzmann distribution, the free electrons are polarized to more than 99% in a ~ 5 T field generated by a pair of superconducting coils and at a ~ 1 K temperature. A radiofrequency field is then applied to induce transitions to states with a preferred nuclear spin orientation. Because the relaxation time of the electrons is much shorter than that of the nuclei, polarized nuclei are accumulated. The electron beam had to be rastered uniformly in a 1 cm radius to minimize local heating and depolarization. A two-magnet chicane compensated for the deflection of the electron beam by the target field. The scattered electrons were detected in the HMS detector and the knocked-out neutrons in a 160×160 cm^2 large scintillator detector, six planes thick, preceded by two planes of thin scintillators serving as veto detectors of charged particles, shielded by a 2.5 cm thick lead curtain from direct gamma rays originating in the target. The measured beam-target asymmetry A_{en}^V , with the target polarization vector in the scattering plane and perpendicular to the momentum transfer vector, can be directly related to the ratio G_E^n/G_M^n

$$A_{en}^V = -\frac{2\sqrt{\tau(\tau+1)}\tan(\theta_e/2)G_E^n/G_M^n}{(G_E^n/G_M^n)^2 + \tau/\epsilon} \quad (10)$$

Corrections for charge-exchange reactions in the target material and in the lead curtain were determined by a Monte-Carlo simulation.

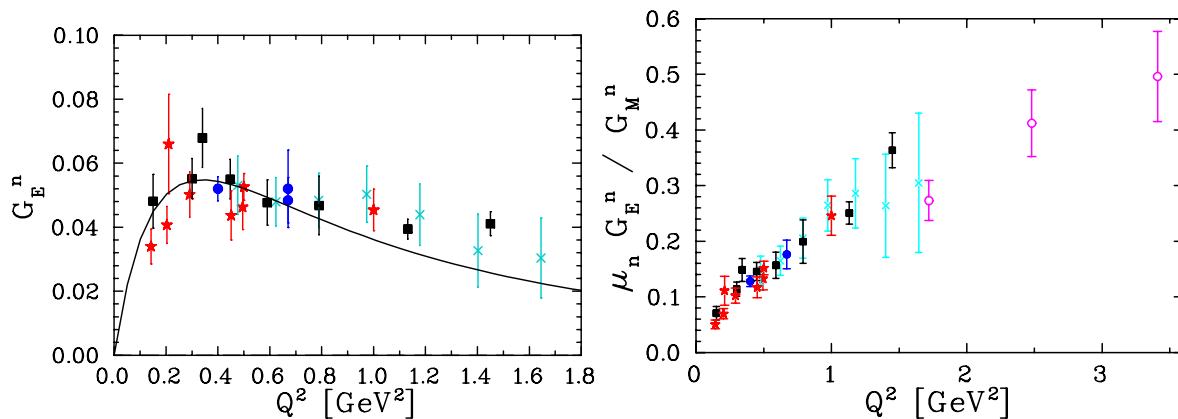


Figure 5. Current status of extractions of G_E^n . Squares are extractions from recoil-polarization measurements on ^2H , stars (circles) are from cross-section asymmetries from polarized ^2H (^3He) targets. The crosses are from a modern analysis of electron-deuteron elastic scattering [62], and the curve represents the Galster fit to G_E^n . Data sets are the same as shown in Ref. [3] with the addition of new results from BLAST [63] (red stars) and the high- Q^2 results from E02-013 (hollow circles).

Figure 5 shows the combined results from all of the high-precision extractions of G_E^n . Results from recoil-polarization measurements on ^2H and cross-section asymmetry measurements from

polarized ^2H and ^3He targets are in good agreement. The limited figure of merit of the polarized ^2H targets, due to restrictions in the polarization, the dilution factor, and the beam current, inhibited its use at higher Q^2 -values.

Experiment E02-013 ran in Hall A in 2006 with a polarized ^3He target, a large-acceptance neutron detector and a large-acceptance electron spectrometer (“BigBite”). The target utilized hybrid optical pumping in which a mixture of rubidium and potassium is used to enhance the spin exchange, resulting in an in-beam polarization of $\sim 50\%$. The BigBite spectrometer consisted of a large dipole magnet with an angular acceptance of close to 100 msr and a momentum acceptance of 90%. Its detector package contained two planes of drift chambers and a lead-glass shower calorimeter. A special target holding field magnet was designed that also provided the required magnetic shielding of the target cell from the fringe field of BigBite. The neutron detector was the largest dedicated neutron detector ever built. It had an active area of $1.6 \times 5 \text{ m}^2$, consisting of 250 scintillators stacked in 7 planes that were interspersed with a 2.5 cm thick iron conversion plane and preceded by 7.5 cm of lead and iron shielding and 2 veto planes made from 200 thin scintillator bars. The use of these three novel devices at a luminosity of $3 \cdot 10^{37} \text{ cm}^{-2}\text{s}^{-1}$ made it possible to extend the G_E^n data set to 3.4 GeV^2 , as shown in the right panel of Fig. 5. Charge-exchange corrections were determined by taking data, in addition to ^3He , on a number of targets with different N/Z ratios, such as hydrogen, deuterium and ^{12}C . Nuclear-medium effects, including pion production, were determined through Glauber-type calculations.

5. Impact of the Jefferson Lab Program

The dramatically improved data set that has become available in the last decade, has had a transformative effect on the study of nucleon form factors. While the issue of two-photon exchange corrections led to a brief period of uncertainty, it soon became clear that the surprising new results on G_E^p/G_M^p were correct and that our textbook picture of the proton form factors would have to be revised. The impact of these new experimental results was magnified by the parallel developments on the theory side, in particular several attempts to learn more about the internal sub-structure of the nucleon within the framework of Generalized Parton Distributions (GPDs).

The most dramatic new result was the fall-off of the ratio G_E/G_M for the proton. One question raised by this striking behavior was whether G_E^p may have a zero crossing at high Q^2 . This possibility was considered rather exotic when the high- Q^2 polarization results were first available, as the idea that G_E^p and G_M^p both followed the dipole form and decreased monotonically towards zero had become common wisdom based on the earlier Rosenbluth measurements. However, there is nothing unusual about a zero crossing in G_E^p . In fact, Dombey stated in a 1969 review article [7] that “As $G_E = F_1 - \tau F_2$, it is *a priori* quite likely that G_E becomes negative for large values of $[Q^2]$ ”. The recent GEp(III) experiment [12] shows a decrease in the fall of G_E^p/G_M^p with Q^2 , suggesting that a zero crossing, if it occurs, is at higher Q^2 than suggested by the earlier measurements. Results from the new G_E^n experiment [64] suggest that G_E^n falls less rapidly, roughly following the dipole form for Q^2 from 1.5 to 3.4 GeV^2 .

The expectation for high Q^2 was that the form factors would behave according to the leading term in perturbative QCD (pQCD). This led to the expectation that the ratio G_E/G_M would become independent of Q^2 at large Q^2 -values (corresponding to $F_1/F_2 \propto Q^2$), as suggested by the older Rosenbluth results. The pQCD predictions were reexamined, and while the leading power behavior yields a constant ratio, there are terms that give a logarithmic Q^2 -dependence that can be large even at the highest Q^2 -values of existing data [65]. Figure 6 shows scaling for the proton and neutron, along with a selection of calculations.

Miller’s calculation [66] is based on an extension of the cloudy bag model, in which three relativistically moving constituent quarks are surrounded by a pion cloud. Roberts [67] solves a Poincare covariant Faddeev equation for dressed quarks in which correlations between those

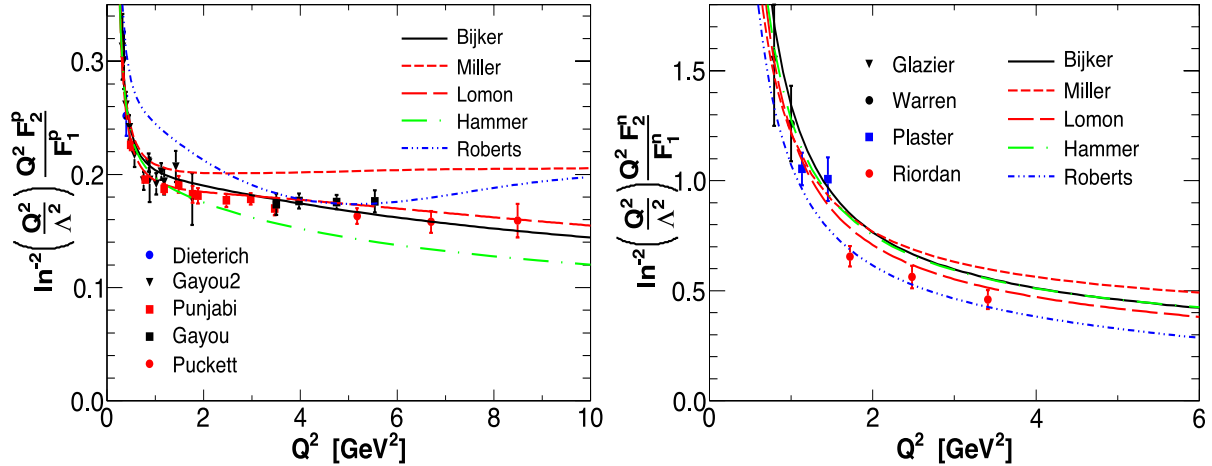


Figure 6. The F_2/F_1 ratio for the proton and neutron, after applying a logarithmic scaling correction from [65], with $\Lambda = 300$ MeV. The proton (left) is consistent with this logarithmic scaling above 1–2 GeV^2 , while the preliminary neutron results, extending up to $Q^2 = 3.4$ GeV^2 , do not yet show the same scaling behavior.

are expressed via diquarks. The other three calculations use different extensions of the Vector Meson Dominance model where the scattering amplitude is expressed in a bare-nucleon form factor, multiplied by the amplitude of the photon interaction with a vector meson. In Bijker and Iachello’s model [68], the virtual photon is assumed to couple to the assumed intrinsic structure of the quarks and one of three vector mesons (ρ , ω and ϕ). By adding more parameters, such as the width of the ρ -meson and the masses of heavier vector mesons, Lomon [69, 70] succeeded in describing all EMFF data. Hammer and Meissner [71] included the isovector $\pi\pi$ channel through dispersion relations. Because the VMD models require a significant number of parameters to provide good fits to the data, they are not expected to have significant predictive power.

While the proton data are consistent with the modified scaling of Ref. [65], the neutron data do not show this scaling, and it has been suggested [3] that the non-perturbative mass scale required for the proton indicates that the perturbative prediction is not applicable in this Q^2 -range. These logarithmic terms are connected to spin-flip contributions, which for nearly massless quarks must come from the orbital angular momentum of the quarks. Quark orbital angular momentum is an important feature in many of the nucleon models that show G_E^p/G_M^p decreasing with Q^2 .

In the Born approximation, the form factors are Fourier transforms of the charge and magnetization distributions in the Breit (center-of-momentum) frame. The extraction of those distributions in the rest frame requires relativistic boost corrections, which scale as Q^2/m^2 . At low Q^2 , the mass of the constituent quarks has evolved to ~ 400 MeV, so the corrections are expected to be relatively small for very low Q^2 -values. Kelly [72] used a simple model for these boost corrections in obtaining the results shown in Fig. 7 for the charge and magnetization distributions of the proton and the neutron. For the proton, the central magnetization density is 50% larger than the central charge density, as a result of its sharper drop-off. For the neutron, there is a positive central charge distribution with an extended negative tail, strongly supporting the picture that the neutron has a (p, π^-) component in its wave function.

In parallel with the improvements in the experimental techniques, new tools were also being developed to allow for the extraction of additional information about the structure of the nucleon. The development of the framework of Generalized Parton Distributions (GPDs) led to

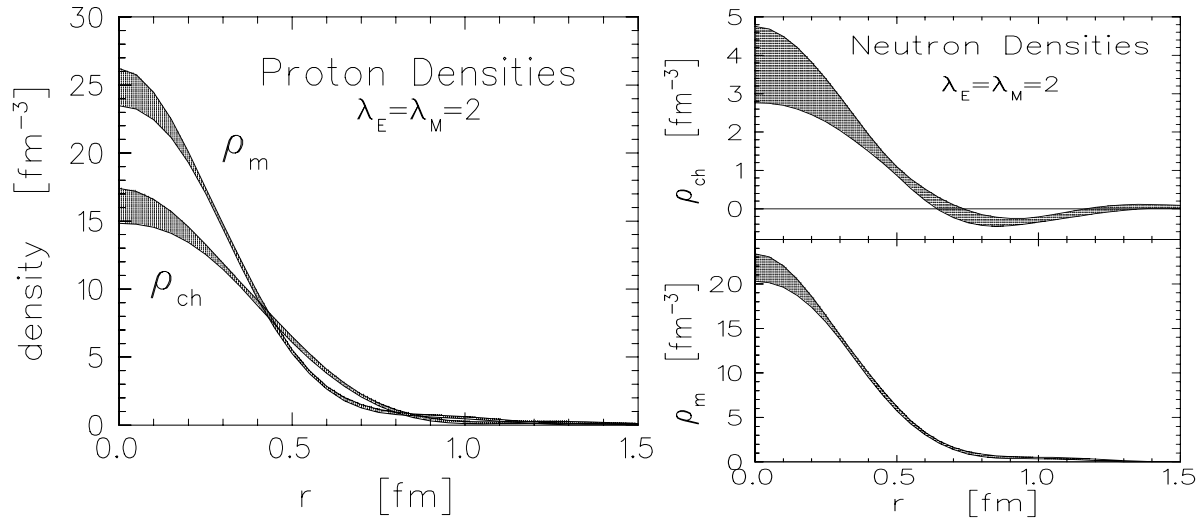


Figure 7. Charge and magnetization densities for the proton and neutron. Figures taken from Ref. [72].

new approaches that go beyond the traditional one-dimensional pictures of the spatial charge distributions and look into correlations in the momentum, space, and spin structure of the quarks in the nucleon. Several groups looked at isolating the spatial distribution for low and high momentum quarks, or for the quarks with spins parallel, anti-parallel, or transverse to the nucleon spin [73, 74], as illustrated in Fig. 8. More recently, both the charge and magnetization densities, along with their uncertainties, has been extracted [75]. The impact of these data on constraining GPDs, and broader discussion of the interpretation of nucleons in terms of the GPDs is included in a later article in this collection [76].

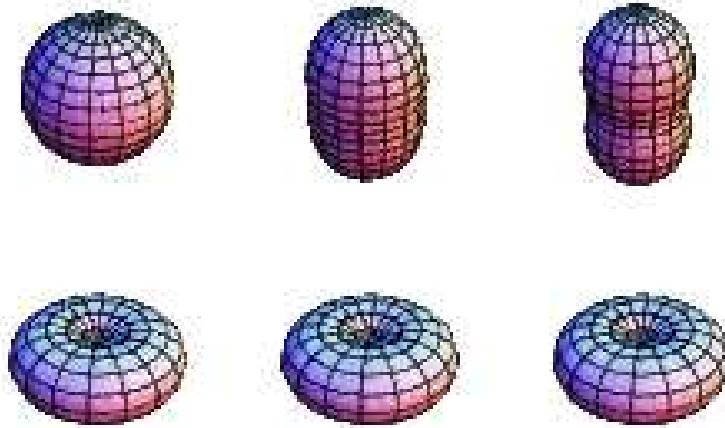


Figure 8. Visualizations of the spatial quark distributions in the proton [73]. The top (bottom) distributions are for quark spin parallel (anti-parallel) to the proton spin. Contours of constant density are shown for quark momenta 0, 1, and 2 GeV/c (from left to right).

The approaches built on GPDs provided more detailed information on nucleon sub-structure, but significant modeling is required to build GPDs from the constraints provided mainly by form

factors and structure functions. Related studies were performed that led to the development of a model-independent procedure to extract information on the spatial distributions that depend only on the form factors as input. Miller [77] showed that in the infinite momentum frame (IMF), the transverse charge distribution as a function of the impact parameter is simply the two-dimensional Fourier transform of the Dirac form factor $F_1(Q^2)$. This provides a model-independent extraction of the transverse spatial distribution of charge for a nucleon in the IMF, which is more closely connected to the quark parton momentum distributions and GPDs. While the proton's transverse charge distribution was consistent with expectations, the neutron yielded a small, negative region of charge in the very center. This novel feature was not consistent with expectations based on simply treating the IMF distribution as the transverse spatial distribution in the rest frame.

The Drell-Yan-West relation links the x -dependence of a parton distribution function $q(x)$ at large x to the Q^2 -dependence of a form factor $F(Q^2)$:

$$q(x) \propto (1-x)^{(\nu-1)} \longleftrightarrow F(Q^2) \propto Q^{-\nu}. \quad (11)$$

The preliminary G_E^n data at large Q^2 show a slower fall-off with Q^2 than the G_E^p data, indicating a dominance of d quarks over u quarks at large x . This observation, first suggested by Kroll [78], is in agreement with the phenomenological modeling of the parton distribution functions, such as CTEQ6M [79]. Using models of neutron GPDs, the correlation between the transverse spatial distributions of the nucleon in the IMF and the quark momenta was examined, and it was shown that this negative central charge in the neutron was the result of this strong d -quark dominance at high x [80]. In the IMF, the center of momentum of the nucleon is the longitudinal momentum weighted average of the transverse quark positions. In the limit where one quark has $x \rightarrow 1$, the position of that single quark provides the dominant contribution in defining the transverse center of the nucleon, and thus contributions from large x become localized near the center of the nucleon. Figure 9 shows the charge density of the neutron coming from different x regions. At low x , the density of up and down quarks is similar, and there is a net positive charge with a broad spatial distribution. At large x , the density of down quarks is more than twice that of up quarks, so the net charge is negative and the distribution becomes more localized, yielding the small negative core in the neutron.

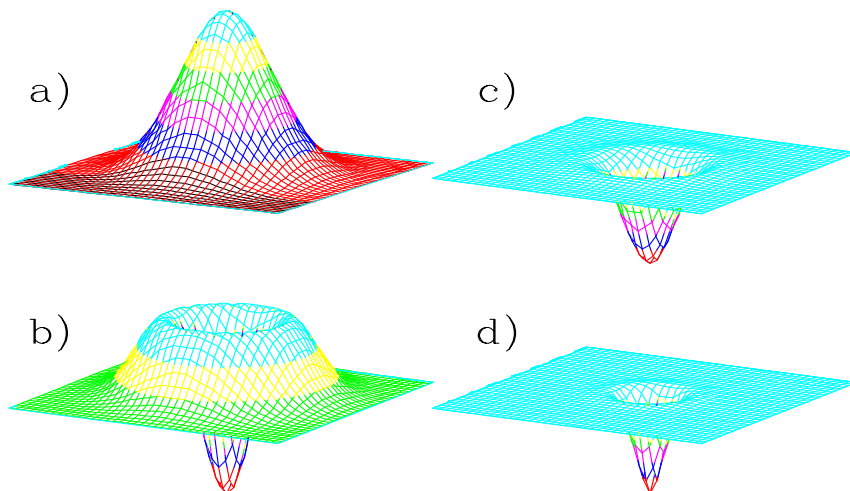


Figure 9. Contributions to the infinite momentum frame transverse charge density of the neutron coming from low (a) to high (d) momentum quarks [80].

Such visualizations of the nucleon charge distributions on the light front have been expanded to the case of nucleons polarized transversely to the light front [81]. Both the (proton and neutron) unpolarized distributions are shifted along the polarization axis due to the nucleon's large anomalous magnetic moment, which results in an induced electric dipole moment perpendicular to the polarization axis.

The new form-factor data provide information on much more than just the spatial structure of the nucleon. The new high- Q^2 measurements, combined with the new, complete set of low- Q^2 form-factor data, provide powerful constraints on models of nucleon structure. Figure 6 shows a small selection of calculations and it is clear that there is a significant scatter even between modern calculations. Prior to the Jefferson Lab program, only G_M^p was known with high precision over a large Q^2 -range; the other form-factor extractions were limited in both precision and kinematic coverage. Many theoretical approaches were used to model nucleon structure and with parameters adjusted to reproduce G_M^p , there were only limited constraints from the other form factors. The improved measurements of G_E^p and G_M^n provided real challenges for calculations that had, until this time, been minimally constrained. High-precision measurements of G_E^n have been more difficult to incorporate in evaluating models of nucleon structure. Pion-cloud contributions are neglected in many calculations, but play an important role in the behavior of G_E^n at low Q^2 . The newest G_E^n measurement extends the data to 3.4 GeV^2 , providing a complete set of form-factor extractions in the Q^2 -region where pion-cloud contributions should be small and the form factor is expected to be sensitive to the quark core of the neutron.

Early experiments on the proton focused on the high- Q^2 region, but precision measurements at low Q^2 also became an area of renewed interest. Had the up and down quark distributions been identical, the neutron would have been neutral everywhere yielding $G_E^n = 0$ at all Q^2 -values. The non-zero values of G_E^n at low Q^2 demonstrate that there is a net positive charge in the core of the neutron and a negative charge distribution on the outside, as expected from virtual fluctuations of the neutron into a proton and a negative pion. An intriguing analysis [26] suggested the possibility that similar contributions may be present in all of the form factors. For the proton, the pion cloud is a small contribution on top of the quark core, and precision data are necessary to test models of pion contributions for all four form factors. New measurements [15, 27] at low Q^2 , shown in Fig. 3 showed hints of structure in the ratio $\mu_p G_E^p / G_M^p$, motivating experiment E08-007, which will cover this Q^2 -range with significantly higher precision.

Having a precise and complete data set at low Q^2 also provides the opportunity to study the contributions of the different quark flavors. Neglecting strange and heavier quarks, the proton and neutron form factors consist of contributions from the up and down quarks. Since many nucleon properties appear to have significant contributions from strangeness, neglecting strange quarks may not be well justified, and additional information is required to constrain the impact of strangeness on the nucleon form factors. Measurements of parity-violating electron scattering can provide information on the coupling of a Z-boson to the proton. This provides a complete set of observables that allows for a separation of the up, down, and strange quark contributions to the nucleon form factors, as discussed in detail in the following article [82]. Data on both proton and neutron are also needed to extract the isovector form factors (proton minus neutron). This is the combination that can be most reliably extracted from lattice QCD calculations, where taking the difference between proton and neutron removes the influence of disconnected diagrams which are difficult to calculate.

Finally, data at even lower Q^2 -values, below 0.1 GeV^2 , can also have an important impact. Extraction of the proton charge radius depends on having reliable measurements of the form factors at extremely low Q^2 , and what we have learned about two-photon exchange corrections has led to an updated extraction of the proton charge radius [83, 84]. Ultra-high precision atomic physics measurements, e.g. hyperfine splitting in hydrogen and muonic hydrogen, are extremely sensitive to proton structure corrections, including terms directly calculated from the

low- Q^2 proton form factors [81]. Future experiments (Table 1) will extend proton form factor extractions down below 0.02 GeV^2 with significantly improved precision over older Rosenbluth experiments.

6. Future Plans and Outlook

State of the art polarized electron beams, coupled with high figure-of-merit polarized targets and recoil polarimeters, have enabled a program of measurements at Jefferson Lab that has dramatically modified our picture of nucleon form factors. Individual experiments, in particular the surprising results of the proton electric form-factor measurements, have led to a reexamination of long held pictures of nucleon structure. Taken together, these experiments have provided data of dramatically improved quality for most form factors over large kinematic ranges, and have led to a resurgence in efforts to evaluate nucleon models against a complete set of form factor measurements. With neutron measurements beginning to cover a significant portion of the Q^2 -range for which precise proton data already exist, we can begin to extract model-independent information about the difference between the up and down quark distributions, and the high- Q^2 extractions of G_E^n show that there is a noticeable difference between the up and down quark spatial distributions in the neutron [64].

These new data, as well as the techniques that made these measurements possible, will continue to have impact on other experimental investigations. Precise knowledge of the electromagnetic form factors is necessary to probe the strange quark contributions to the nucleon using parity-violating lepton scattering [82]. It is also important input to high-precision nuclear structure measurements that utilize quasi-elastic scattering from the nucleus, and measurements of hyperfine splitting in hydrogen. In addition, the measurement of nucleon form factors utilizing polarization measurements allows for much more sensitive investigations into the effect of the nuclear medium on the nucleon form factors. The comparison of free to bound proton form factors, using polarization transfer in quasi-elastic scattering from ^4He [85, 86], yields smaller corrections than similar measurements that relied on Rosenbluth separations, although the impact of these corrections on the interpretation is a topic of great interest [87].

Soon, the last of the measurements from Table 1 will be completed as the 6 GeV program is brought to a close. The increased electron energies available after the 12 GeV upgrade, coupled with further improvements in the experimental equipment, will enable a dramatic extension of the program presented here, doubling or tripling the Q^2 range of most of these measurements. This will provide valuable constraints on generalized parton distributions, an important focus of the upgrade, at very high Q^2 values. In addition to the benefits gained by extending the Q^2 -range for the individual form factors, this will also provide a complete set of form factor measurements at large Q^2 , where the pion-cloud contributions are expected to be small and the measurements can be directly compared to calculations of the quark core of the nucleon. This will make evaluation of nucleon models more reliable, as pion-cloud contributions are typically difficult to include in a self-consistent fashion.

Acknowledgments

This work was supported by the Department of Energy, Office of Nuclear Physics, contract nos. DE-AC05-84ER40150 and DE-AC02-06CH11357 and by the National Science Foundation, grant PHY-0753777. The authors thank those of their colleagues who assisted in the preparation of this overview and apologies for omissions made necessary by the constraints of length and time.

References

- [1] C. E. Hyde-Wright and K. de Jager, *Ann. Rev. Nucl. Part. Sci.* **54**, 217 (2004).
- [2] C. F. Perdrisat, V. Punjabi and M. Vanderhaeghen, *Prog. Part. Nucl. Phys.* **59**, 694 (2007).
- [3] J. Arrington, C. D. Roberts and J. M. Zanotti, *J. Phys.* **G34**, S23 (2007).

- [4] S. Platchkov *et al.*, Nucl. Phys. **A510**, 740 (1990).
- [5] A. I. Akhiezer, L. N. Rozentsweig and I. M. Shmuskevich, Sov. Phys. JETP **6**, 588 (1958).
- [6] A. I. Akhiezer and M. P. Rekalov, Sov. Phys. Dokl. **13**, 572 (1968).
- [7] N. Dombey, Rev. Mod. Phys. **41**, 236 (1969).
- [8] R. G. Arnold, C. E. Carlson and F. Gross, Phys. Rev. C **23**, 363 (1981).
- [9] V. Punjabi *et al.*, Phys. Rev. C **71**, 055202 (2005), erratum-ibid. C71:069902, 2005.
- [10] M. K. Jones *et al.*, Phys. Rev. Lett. **84**, 1398 (2000).
- [11] O. Gayou *et al.*, Phys. Rev. Lett. **88**, 092301 (2002).
- [12] A. J. R. Puckett *et al.*, Phys. Rev. Lett. **104**, 242301 (2010).
- [13] J. Arrington, Phys. Rev. C **69**, 022201(R) (2004).
- [14] I. A. Qattan *et al.*, Phys. Rev. Lett. **94**, 142301 (2005).
- [15] C. B. Crawford *et al.*, Phys. Rev. Lett. **98**, 052301 (2007).
- [16] M. Paolone, S. Malace, S. Strauch, I. Albayrak, J. Arrington *et al.*, Phys.Rev.Lett. **105**, 072001 (2010).
- [17] X. Zhan *et al.*, *arXiv:nucl-ex/1102.0318* (2011).
- [18] G. Ron *et al.*, *to be submitted to Phys. Rev. C* (2011).
- [19] J. J. Kelly, Phys. Rev. C **70**, 068202 (2004).
- [20] J. Arrington, W. Melnitchouk and J. A. Tjon, Phys. Rev. **C76**, 035205 (2007).
- [21] J. Arrington, Phys. Rev. C **68**, 034325 (2003).
- [22] M. E. Christy *et al.*, Phys. Rev. C **70**, 015206 (2004).
- [23] A. Afanasev, I. Akushevich and N. Merenkov, Phys. Rev. **D64**, 113009 (2001).
- [24] L. C. Maximon and J. A. Tjon, Phys. Rev. C **62**, 054320 (2000).
- [25] P. A. M. Guichon and M. Vanderhaeghen, Phys. Rev. Lett. **91**, 142303 (2003).
- [26] J. Friedrich and T. Walcher, Eur. Phys. J. **A17**, 607 (2003).
- [27] G. Ron *et al.*, Phys. Rev. Lett. **99**, 202002 (2007).
- [28] J. Bernauer *et al.*, Phys.Rev.Lett. **105**, 242001 (2010).
- [29] P. G. Blunden, W. Melnitchouk and J. A. Tjon, Phys. Rev. Lett. **91**, 142304 (2003).
- [30] J. Arrington, Phys. Rev. C **69**, 032201(R) (2004).
- [31] J. Arrington, Phys. Rev. C **71**, 015202 (2005).
- [32] M. Meziane *et al.*, *arXiv:nucl-ex/1012.0339* (2010).
- [33] J. Guttman, N. Kivel, M. Meziane and M. Vanderhaeghen, *arXiv:hep-ph/1012.0564* (2010).
- [34] D. Borisyuk and A. Kobushkin, *arXiv:hep-ph/1012.3746* (2010).
- [35] C. E. Carlson and M. Vanderhaeghen, Ann. Rev. Nucl. Part. Sci. **57**, 171 (2007).
- [36] P. G. Blunden, W. Melnitchouk and J. A. Tjon, Phys. Rev. C **72**, 034612 (2005).
- [37] S. Kondratyuk and P. G. Blunden, Phys. Rev. C **75**, 038201 (2007).
- [38] Y. C. Chen, A. Afanasev, S. J. Brodsky, C. E. Carlson and M. Vanderhaeghen, Phys. Rev. Lett. **93**, 122301 (2004).
- [39] A. V. Afanasev, S. J. Brodsky, C. E. Carlson, Y.-C. Chen and M. Vanderhaeghen, Phys. Rev. D **72**, 013008 (2005).
- [40] A. V. Afanasev, I. Akushevich and N. P. Merenkov, Phys. Rev. **D65**, 013006 (2002).
- [41] Y. M. Bystritskiy, E. A. Kuraev and E. Tomasi-Gustafsson, Phys. Rev. **C75**, 015207 (2007).
- [42] A. V. Afanasev, *Proceedings of the International Workshop on Exclusive Reactions at High Momentum Transfer, 21-24 May 2007, Jefferson Lab. arXiv:hep-ph/0711.3065* (2008).
- [43] L. W. Mo and Y.-S. Tsai, Rev. Mod. Phys. **41**, 205 (1969).
- [44] V. Tvaskis *et al.*, Phys. Rev. C **73**, 025206 (2006).
- [45] L. Pentchev, AIP Conf. Proc. **1056**, 357 (2008).
- [46] J. Arrington, D. M. Nikolenko *et al.*, Proposal for positron measurement at VEPP-3, nucl-ex/0408020.
- [47] J. Arrington, AIP Conf. Proc. **1160**, 13 (2009), 0905.0713.
- [48] B. Anderson *et al.*, Phys. Rev. C **75**, 034003 (2007).
- [49] H. Anklin *et al.*, Phys. Lett. **B428**, 248 (1998).
- [50] G. Kubon *et al.*, Phys. Lett. **B524**, 26 (2002).
- [51] J. Lachniet *et al.*, Phys. Rev. Lett. **102**, 192001 (2009).
- [52] S. Jeschonnek and J. W. Van Orden, Phys. Rev. C **62**, 044613 (2000).
- [53] W. Xu *et al.*, Phys. Rev. Lett. **85**, 2900 (2000).
- [54] W. Xu *et al.*, Phys. Rev. C **67**, 012201 (2003).
- [55] J. Alcorn *et al.*, Nucl. Inst. & Meth. **A522**, 294 (2004).
- [56] J. Golak, G. Ziemer, H. Kamada, H. Witala and W. Gloeckle, Phys. Rev. C **63**, 034006 (2001).
- [57] R. Madey *et al.*, Phys. Rev. Lett. **91**, 122002 (2003).
- [58] B. Plaster *et al.*, Phys. Rev. **C73**, 025205 (2006).
- [59] G. Warren *et al.*, Phys. Rev. Lett. **92**, 042301 (2004).

- [60] D. G. Crabb and D. B. Day, Nucl. Instrum. Meth. **A356**, 9 (1995).
- [61] T. D. Averett *et al.*, Nucl. Instrum. Meth. **A427**, 440 (1999).
- [62] R. Schiavilla and I. Sick, Phys. Rev. C **64**, 041002(R) (2001).
- [63] E. Geis *et al.*, Phys. Rev. Lett. **101**, 042501 (2008).
- [64] S. Riordan *et al.*, Phys. Rev. Lett. **105**, 262302 (2010).
- [65] A. V. Belitsky, X.-d. Ji and F. Yuan, Phys. Rev. Lett. **91**, 092003 (2003).
- [66] G. A. Miller, Phys. Rev. C **66**, 032201 (2002).
- [67] I. C. Cloet, G. Eichmann, B. El-Bennich, T. Klahn and C. D. Roberts, Few Body Syst. **46**, 1 (2009).
- [68] R. Bijker and F. Iachello, Phys. Rev. C **69**, 068201 (2004).
- [69] E. L. Lomon, Phys. Rev. C **66**, 045501 (2002).
- [70] E. L. Lomon, *arXiv:nucl-th/0609020* (2006), [nucl-th/0609020](#).
- [71] H. W. Hammer and U.-G. Meissner, Eur. Phys. J. **A20**, 469 (2004).
- [72] J. J. Kelly, Phys. Rev. C **66**, 065203 (2002).
- [73] G. A. Miller, Phys. Rev. C **68**, 022201 (2003).
- [74] A. V. Belitsky, X.-d. Ji and F. Yuan, Phys. Rev. **D69**, 074014 (2004).
- [75] S. Venkat, J. Arrington, G. A. Miller and X. Zhan, Phys. Rev. C **83**, 015203 (2011).
- [76] C. E. Hyde, M. Guidal and A. V. Radyushkin, *Deep Virtual Exclusive Processes and Generalized Parton Distributions*, this volume, 2011.
- [77] G. A. Miller, Phys. Rev. Lett. **99**, 112001 (2007).
- [78] P. Kroll, *Proceedings of the International Workshop on Exclusive Reactions at High Momentum Transfer, 21-24 May 2007, Jefferson Lab. arXiv:hep-ph/0710.2771* (2008).
- [79] J. Pumplin *et al.*, JHEP **07**, 012 (2002).
- [80] G. A. Miller and J. Arrington, Phys. Rev. **C78**, 032201 (2008).
- [81] C. E. Carlson, V. Nazaryan and K. Griffioen, [arXiv:physics.atom-ph/0805.2603](#) (2008), [0805.2603](#).
- [82] K. Paschke, A. Thomas, R. Michaels and D. Armstrong, *Strange Vector Form-Factors from Parity-Violating Electron Scattering*, this volume, 2011.
- [83] R. Rosenfelder, Phys. Lett. B **479**, 381 (2000).
- [84] P. G. Blunden and I. Sick, Phys. Rev. C **72**, 057601 (2005).
- [85] S. Strauch *et al.*, Phys. Rev. Lett. **91**, 052301 (2003).
- [86] W. K. Brooks, S. Strauch and K. Tsushima, *Medium Modifications of Hadron Properties and Partonic Processes*, this volume, 2011.
- [87] R. Schiavilla, O. Benhar, A. Kievsky, L. E. Marcucci and M. Viviani, Phys. Rev. Lett. **94**, 072303 (2005).